Optimal Filtering and Design of Photon Pair Sources in the Presence of Background Noise Photons

Jordan M. Thomas*,[1] Andrew R. Cameron*,[2] Akil Pathiranage,[2] Si Xie,[2,3] Raju Valivarthi,[3,4] Panagiotis Spentzouris,[2] Maria Spiropulu,[3,4] Cristián Peña,[2] and Prem Kumar[1,5]

[1] *Center for Photonic Communication and Computing, Northwestern University, 2145 Sheridan Road, Evanston, Illinois 60208, USA*
[2] *Fermi National Accelerator Laboratory, Batavia, IL 60510, USA*
[3] *Division of Physics, Mathematics and Astronomy, California Institute of Technology, Pasadena, CA 91125, USA*
[4] *Alliance for Quantum Technologies (AQT), California Institute of Technology, Pasadena, CA 91125, USA*
[5] *Department of Physics and Astronomy, Northwestern University, 2145 Sheridan Road, Evanston, Illinois 60208, USA*

(Dated: May 23, 2025)

Noise photons from classical communications in optical fibers, from ambient light in free space, and from inelastic scattering of pump light in some photon pair and frequency conversion devices impose challenges for high-fidelity quantum applications using single-photon-level signals. Filtering is necessarily performed in nearly all of these experiments, yet narrow spectral filtering is well known to cause an inherent reduction in heralding efficiency for most photon-pair sources using spontaneous parametric down-conversion and four-wave mixing. Here, we experimentally and theoretically explore the filtering of photon pairs in noisy environments. Using tunable spectral filters, low-jitter detectors, and polarizers, we investigate the filtering of spontaneous Raman scattering (SpRS) noise photons occurring when quantum networks coexist with classical communications in single-mode fibers. We find that reduced filter heralding efficiency due to tight spectral filtering of a photon pair's joint spectral intensity (JSI) can limit the ability to improve fidelity, indicating an additional consideration for optimal source and receiver design beyond single-photon filtering. In fact, such effects impact visibility excluding additional noise due to multi-pair emission outside of the overlap of each filter on the source's JSI. Accordingly, the optimal visibility is dictated by the the inherent phase-matching conditions, the pump spectral bandwidth, signal-idler filter bandwidth, and mean photon number. This leads to the potential trade-off between visibility and spectral purity, consequential for applications requiring the interference of independent photons (e.g., teleportation, swapping, etc.), pulsed high-rate quantum sources and/or time-bin encoding. As a proof-of-principle experiment, we distribute C-band time-bin entangled photons each over 25-km spools alongside 10-Gbps C-band classical communications, which introduces high SpRS noise due to the C-band/C-band wavelength allocation. Using narrow filtering, we distribute spectrally pure photons capable of performing quantum key distribution over 50-km total fiber with record launch powers (-2.2 dBm) and project that classical data rates exceeding terabits/s could be achieved using modern classical methods.

PACS numbers: 47.15.-x

I. INTRODUCTION

Quantum optical applications operating in the single-photon regime are inherently susceptible to any degree of background noise due to weak signals arriving at single-photon detectors. Noise photons can be introduced when going beyond proof-of-principle laboratory experiments and into real world conditions, such as spontaneous Raman scattering (SpRS) generated by classical telecommunications propagating in an optical fiber [1–7], ambient light in free-space communications [8], and SpRS noise photons generated inside spontaneous four-wave mixing (SFWM) photon-pair sources [9], or during quantum frequency conversion [10–13].

For background noise photons that are randomly distributed in frequency, time, polarization, and spatial modes, filtering can be applied around the quantum signal's modes to minimize the passing of background noise into detectors. Single-photon quantum applications applying incoherent spectro-temporal filtering are eventually limited by the filter's time-bandwidth product. As we will show, the filtering of two-photon states originating from spontaneous parametric down-conversion (SPDC) or SFWM processes have additional limits due to the physics of narrowly filtering their joint spectral amplitude (JSA). This is due to the fact that narrowly filtering the JSA of a source, more commonly used to erase spectral entanglement to obtain spectrally pure photons,

This manuscript has been authored by FermiForward Discovery Group, LLC under Contract No. 89243024CSC000002 with the U.S. Department of Energy, Office of Science, Office of High Energy Physics.

results in a reduction in heralding efficiency even with perfect insertion loss and detection efficiency [14]. This is because as one cuts into the JSA, the signal and idler filters do not entirely overlap with their pair along the unfiltered JSA, leading to signal/idler single-photon detections that do not result in true coincidences with their pair. To the best of our knowledge, the impact of this phenomenon on quantum applications needing narrow filtering in noisy media has yet to be investigated.

In this paper, we explore the filtering of photon pairs in frequency, time, and polarization via theoretical modeling and experimental investigation. We demonstrate that narrow filtering of the source's JSA places a limit on the ability to improve performance via spectral filtering, even if the time-frequency filtering of each individual photon is not time-bandwidth limited. As a consequence, we discover that optimal performance requires engineering of the source JSA, such as the pump spectral bandwidth and phase-matching angle. For a fixed coincidence detection window, we find that longer-duration pump pulses (100-ps regime) and narrow filtering (10's of picometers) can outperform systems using short pump pulses (1-10's of picoseconds) since a reduced coincidence probability occurs at wider filter bandwidths wherein each detector has a higher noise count probability. For a variable coincidence window, depending on the photon pulse duration, we find that any pump pulse duration can achieve the same CAR, but requires tailoring of the filter bandwidth based on the pump pulse duration and requires access to low-jitter detectors in the short pulse limit. We further investigate the impact of SPDC/SFWM photon statistics to account for multi-pair emission noise, where we find that achieving optimal fidelity requires balancing the increase of source intensity to overcome noise/loss whilst preventing strong multi-pair emission noise in the high-gain regime.

We experimentally study these concepts in the context of integrating quantum and classical communications in optical fiber networks. We transmit wavelength-degenerate 1536.5-nm (DWDM channel 51) photon pairs produced by type-II SPDC to co-propagate in 25km/25 km fiber spools with 10-Gbps C-band data signals at a wavelength of 1547.72 nm (DWDM channel 37). Operating near −10 dBm-level launch powers, this classical light pumps the SMF to generate strong background SpRS noise due to the closely spaced quantum/classical frequency channel difference, with 25km-length fibers generating nearly the highest SpRS strength [2, 15]. We investigate frequency filtering including the regime where JSA effects occur and show the deviation from our model not accounting for these effects. We then investigate temporal filtering and polarization filtering including the impact of not actively tracking time-dependent changes

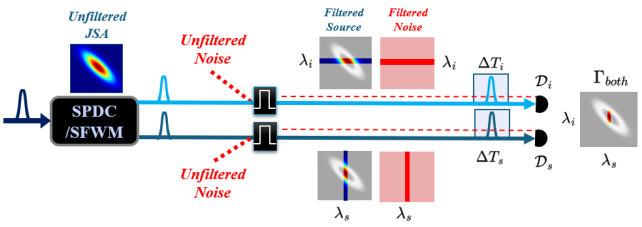

FIG. 1: Conceptual diagram for filtering a photon pair's joint spectral correlations in the presence of background noise photons.

in fiber birefringence. Lastly, we demonstrate time-bin entanglement distribution coexisting with ≈ -2.2 dBm launch power classical data sent over each of the 25 km/25 km fibers. Successful time-bin entanglement distribution with visibilities capable of performing QKD ($> 81\%$) over 100km with 10Gbps classical communications sent over the fiber is demonstrated, showing a record for entanglement distribution for C-band/C-band coexistence of quantum/classical wavelengths. We estimate that using optimal parameters, terabits per second classical data could be transmitted alongside our time-bin entangled pairs whilst maintaining visibilities capable of achieving positive key rates.

This work is consequential for experiments requiring the narrow filtering of both photons either to reduce noise or to obtain spectrally pure photons, for example when classical communications is present in entanglement-based [4, 5, 16] and quantum teleportation-based optical fiber networks [7, 17] or in free-space [18], SpRS generated in SFWM photon-pair sources [9], or storing entangled photons in quantum memories using QFC [10–12]. This work can help guide optimal source and receiver designs to achieve spectrally pure sources and high-rate entanglement-based quantum communications in noisy environments, since short pulses are needed to reach GHz-level repetition rates. Narrow spectral filtering of photon-pair sources is often needed regardless to obtain spectrally pure (single-mode) photons from originally spectrally-entangled JSAs to achieve applications requiring Hong-Ou-Mandel (HOM) interference such as Bell state measurements for quantum teleportation, entanglement swapping, multi-particle entanglement, and beyond. Thus, for experiments such as quantum teleportation alongside classical communications in optical fiber or in free-space, the need for narrow spectral filtering is often two-fold.

II. MODEL

The scenario we explore is pictorially represented in Fig. 1, which shows the filtering of a source's JSA using narrowband filters. In this case, not all detected photons in each arm lead to coincidences due to spectral incompatibility, leading to a reduction in heralding efficiency or coincidence probably. We also plot noise on top of this to show that noise will scale linearly with the filter bandwidth/coincidence window; however, the reduction in coincidence probability of source photons will decrease more rapidly than the noise rejection, limiting the ability to improve fidelity.

The typical way to model photon-pair experiments is to model both the single-photon count probability S_j for signal ($j = s$) and idler ($j = i$) detectors as well as the coincidence count probability C, then quantify the performance via the coincidence-to-accidental ratio (CAR) or visibility V. The typical equations for modeling singles counts S_j and the maximum coincidence counts C, assuming the mean number of generated photons per pulse $\mu \ll 1$ and the true channel efficiency $\eta_j \ll 1$, are $S_j = \mu\eta_j + \mathcal{D}$ and $C = \mu\eta_s\eta_i + A$ [19]. Here, $\mathcal{D}$ is the total background noise count probability and $A = S_sS_i$ is the accidental count probability, or the probability of getting a coincidence detection between two completely independent two-mode squeezed vacuum states (TMSVs), such as neighboring pulse time-slots in a pulse train or when projecting onto orthogonal states of an entangled source's qubit modes. However, this model neglects the properties of the source's JSA as well as situations in which signal and idler photons are filtered with different spectral bandwidths.

Instead, we expand the approach in ref. [14] to include a background noise count probability. Ref. [14] defines the singles count probability as $S_j = n\eta_j\Gamma_j$, where n is the mean number of photons per pulse generated across the entire unfiltered JSA, η_j is the "true" channel j transmission (not accounting for reduced heralding efficiency), and Γ_j is the overlap of the signal/idler spectral filter passband with the JSA given by (see Appendix)

$$\Gamma_j = \iint d\omega_s d\omega_i \left| f\left(\omega_s, \omega_i\right) g_j\left(\omega_j\right)\right|^2,$$

where $f(\omega_s, \omega_i)$ is the unfiltered JSA with $\iint d\omega_s d\omega_i \left| f\left(\omega_s, \omega_i\right)\right|^2 \equiv 1$ and $g_j\left(\omega_j\right)$ is the signal ($j = s$) or idler ($j = i$) normalized filter transmission function.

Expanding this model to include background noise, we model the singles counts in each detector as

$$S_j = n\eta_j\Gamma_j + \mathcal{D}_j. \tag{1}$$

The maximum coincidence probability, assuming $n \ll 1$, is modeled by

$$C \approx \Gamma_{both} n\eta_s\eta_i + A, \tag{2}$$

where Γ_{both} is the probability that both signal and idler photons pass their respected filters and are detected in coincidence, assuming unit transmission, and is derived from the model of the overlap of the filters in the source's unfiltered JSA (see Appendix)

$$\Gamma_{both} = \iint d\omega_s d\omega_i \left| f\left(\omega_s, \omega_i\right) g_s\left(\omega_s\right) g_i\left(\omega_i\right)\right|^2.$$

This is the key parameter in evaluating the effects of reduced coincidence probability relative to the singles counts of both photon pairs and noise. The filter heralding efficiency can then be defined as $\delta_{s/i} = \Gamma_{Both}/\Gamma_{i/s}$ [14].

In the above equations, $\mathcal{D}$ is the noise count probability per time window in which the detector is "open", ΔT. We consider some arbitrary noise photon sources, $\mathcal{R}_j$ that are both random in time and frequency relative to the quantum source photons and has units of $\mathrm{pm}^{-1}\mathrm{s}^{-1}$. For most cases using narrow filtering (< 1 nm), the noise count probability is approximately constant across the filter passband such that we can write the simplified equation for the total background noise count probability $\mathcal{D}$ as

$$\mathcal{D}_j = (\mathcal{R}_j\Delta\lambda_j + d_j)\Delta T_j, \tag{3}$$

where $\Delta\lambda_j$ is the bandwidth of the spectral filter in channel j and d_j is the probability of dark count detection per time ΔT_j. We assume at present that ΔT is greater than the coherence time of the photons. The detector dark counts d are in units of counts/s such that both background noise photons and intrinsic detector dark counts are filtered in the time-domain, whereas only noise generated before detection is spectrally filtered.

The accidental coincidences are still modeled as $A = S_sS_i$, where the signal-to-noise ratio of two-photon experiments can be characterized by the coincidence-to-accidental ratio $CAR = C/A$ or with the non-local two-photon interference fringe visibility of an entangled pair source $V_{ent} = (C - A)/(C + A)$.

We also model the spectral purity, P, as a function of filtering using the approach in [20, 21] to relate the ability to achieve a high CAR or V to the ability to perform interference between independent photons in HOM interference-based applications (see Appendix).

To arrive at equations similar to the typical equations that exclude properties of the JSA or reduced filter

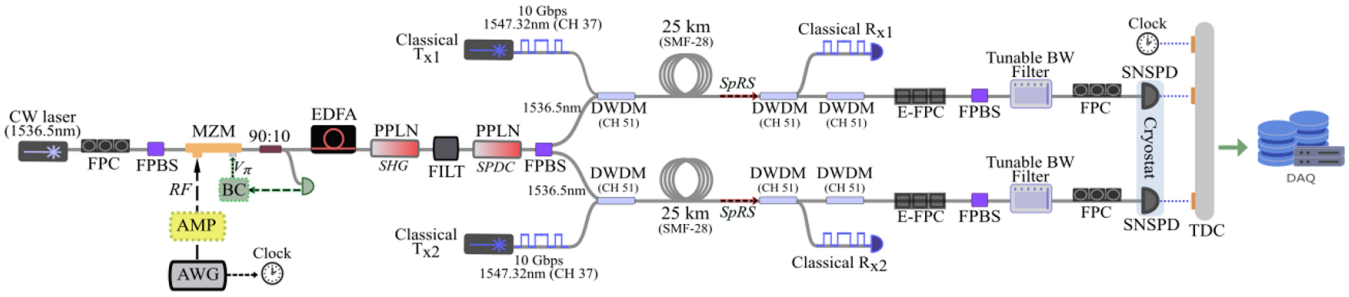

FIG. 2: (a) Experimental diagram. We study filtering spontaneous Raman scattering (SpRS) noise photons when distributing photon pairs generated by type-II SPDC at degenerate wavelengths (1536.5 nm) over 25-km spools to co-propagate with 10-Gbps classical communications operating at 1547.72 nm. The C-band/C-band wavelength allocation generates strong Raman scattering noise that needs to be tightly filtered to perform quantum experiments. The photons are pumped by driving a 20-GHz bandwidth electro-optic modulator by an AWG creating pulses at a 200-MHz repetition rate. The pulse width of the RF signal from the AWG which drives the pump modulator is tuned from 44 ps to 320 ps depending on the experiment. We filter SpRS noise using tunable bandwidth filters in each channel within a range of 32 pm to 600 pm. The lower tuning range allows us to filter below the coherence time of the pump to obtain high spectral purity, at the expense of reduced coincidence count probability. Temporal filtering is performed using low-jitter superconducting nanowire single-photon detectors (SNSPDs) and a time-to-digital converter (TDC) (≈45 ps). Singles counts are monitored to perform active correction of the clock phase for time-dependent drifts in arrival time to allow tight filtering, and polarization is kept filtered using maximized singles using electronic fiber polarization controllers (E-FPCs).

heralding efficiency, we define the mean number of photons per pulse in signal/idler channels after filtering as $\mu_j = n\Gamma_j$, which means signal and idler modes can have different values if the filtering is asymmetric ($\mu_s \neq \mu_i$). If we approximate $\Gamma_s \approx \Gamma_i$, which results in $\delta \equiv \delta_s = \delta_i$, then

$$C \approx \delta\eta_s\eta_i\mu_c + A \tag{4}$$

If $\delta = 1$, we obtain $C = \mu\eta_s\eta_i + A$ and $S_j = \mu\eta_j + \mathcal{D}_j$. We note that this allows approximating μ experimentally as $\mu = \delta_{s,i}S_sS_i/C$ as in [22], however this does not hold for $\Gamma_s \neq \Gamma_i$ (asymmetric filtering or for JSAs with different phase matching angles). We assume our sources are operated in the low gain regime where $\mu \ll 1$ and therefore photon statistics follow a Poisson distribution.

III. EXPERIMENT

Our experimental design is shown in Fig. 2. We study the effects of filtering in the context of coexisting quantum and classical optical communications in standard single-mode fiber (SMF-28). It is well known that allocating quantum and classical channels in nearby wavelength channels, such as both populating C-band DWDM channels, creates very strong SpRS as a function of classical launch power [2, 15]. To study a case in which two photons are transmitted over a noisy medium, we generate C-band photon pairs using SPDC and multiplex them into fibers using dense-wavelength-division multiplexers (DWDMs) to co-propagate over 25km/25km spools with 1547.72-nm classical communications at a rate of 10 Gbps. We either pump our SPDC source with single pulses to create correlated photon pairs or with two pulses to create the time-bin entangled Bell state $|\Phi^+\rangle = \frac{1}{\sqrt{2}}(|EE\rangle + |LL\rangle)$.

The classical signal generates SpRS noise in the quantum signal passband creating the high noise photon environment used to evaluate various methods of filtering. To apply each of the filtering methods, we use tunable bandwidth optical filters (EXFO) with a tuning range of 32pm to 600pm, temporal filtering using a variable coincidence detection window on the output count timestamps of our superconducting nanowire single-photon detectors (Quantum Opus) and time-tagging electronics (Swabian Timetagger Ultra). Each has a temporal jitter of 40ps and 8ps, respectively, allowing tight temporal filtering around the pulses arriving at each detector. At the end of the fibers we include fiber polarizing beam splitters (FPBSs) to apply polarization filtering to prevent $\sim 50\%$ of the SpRS noise from entering each detector, which is possible due to the largely unpolarized SpRS photons over long-distance fiber links [4, 7, 23]. Since long-distance fibers have time-dependent birefringence due to tempurature and mechanical disturbances, active feedback is needed to compensate this effect to align the photon pairs to the polarizing axis of the PBS. We perform this using maximization of single-photon counts in each detector by adjusting the voltages on fiber squeez-

ers in electronic fiber polarization controllers (EFPCs) which keeps each photon aligned to the polarizing axis.

To create our C-band quantum signals, we utilize type-II spontaneous parametric down conversion in a periodically poled lithium niobate (PPLN) waveguide to create wavelength-degenerate pairs of photons at 1536.5 nm. Our source is pumped at a clock rate of 200 MHz by intensity modulating a 1536.5-nm continuous-wave laser (Pure Photonics) using a Mach-Zehnder modulator (Exail). The modulator is driven by radio frequency signals originating from an arbitrary waveform generator (Tektronix). The AWG can be programmed to have a minimum pulse width of 44ps, allowing us to create pulses with a broad spectral bandwidth relative to the lower range of our tunable bandwidth optical filters.

The telecom-band pump pulses are then amplified using an erbium-doped fiber amplifier (EDFA) and injected into a PPLN-WG to undergo second harmonic generation (SHG), producing pulses at 768 nm. These pulse then pump a second PPLN-WG to undergo type-II SPDC, generating degenerate pairs at 1536.5-nm. The signal/idler photons are then separated using a PBS and subsequently multiplexed with the 10 Gbps C-band classical data to co-propagate over 25km fiber spools.

These signals are produced by small-form programmable (SFP) transceivers controlled by a FPGA to generate pseudo-random data. The SFP receiver requires a minimum received power of $P_R = -18$dBm to achieve error-free 10 Gbps communications, dictating a launch power of ≈-13 dBm into the 25-km fiber spools. Due to the close spacing between our quantum and classical wavelengths (∼10 nm), the C-band/C-band wavelength allocation results in a substantial amount of background SpRS noise, allowing us to investigate filtering in very high-noise environments.

The measured joint spectral intensity (JSI) of our source when pumped by a 50-ps duration pump pulse is shown in Fig. 3, which is pre-filtered by a 100-GHz channel spacing DWDM. By overlaying a 50pm spectral passband over the JSI, which is the narrowest filtering we investigate experimentally, it is clear that we can cut into the JSI to achieve spectrally pure photons at the expense of reduced heralding efficiency. This allows us to explore the regime in which narrow filtering is used to both reject background noise photons and increase the source's spectral purity for multi-photon interference.

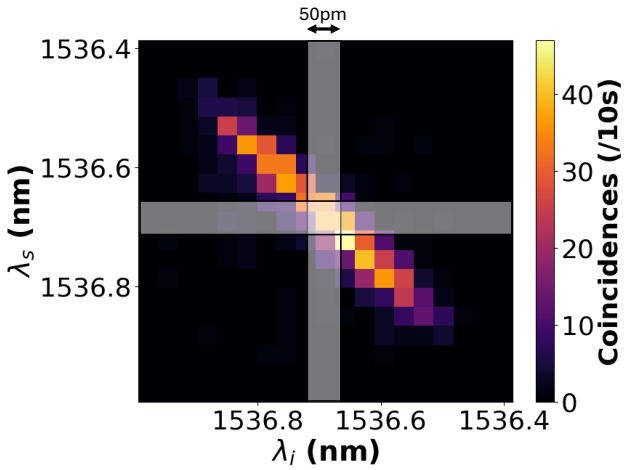

FIG. 3: Measured joint spectral intensity of photon-pairs generated from SPDC with a pump pulse 50-ps FWHM in duration. Photons are prefiltered with 100-GHz channel spacing DWDMs. A 50pm semi-transparent overlay is added at the center wavelength of each photon for a visual reference of the tightest filtering setting used experimentally.

IV. SPECTRAL FILTERING OF PHOTON PAIRS AND BACKGROUND NOISE

A. Comparison between filtering single and two-photon quantum states

To demonstrate the impact of filtering narrow into the source's joint spectrum and how the physics of two-photon filtering differs from single-photon filtering, we study two cases in which one scenario has a wider bandwidth (300pm) and one which has a narrower BW (50pm). We set the time filtering at each detector to maintain the same single-channel time-bandwidth product of the filtering. Since the noise-count probability in each detector is $\propto \Delta\lambda\Delta T$, keeping this fixed should produce the same signal-to-noise ratio in a given detector. However, we will show that this is not necessarily true for CAR in two-photon quantum state experiments when one can not neglect the reduction in coincidence probability from tight filtering.

For the 300pm case, we set a coincidence window of T = 300ps. For the 50pm spectral filtering, we choose T = 1800ps to maintain the same time-BW product of the time-frequency filtering. We also explore how the photon statistics of SPDC/SFWM influence CAR in the two cases, as increasing the source intensity will generate more multi-photon pairs which will reduce the CAR in addition to our background noise. To do this, we plot the CAR for each time-frequency filtering case as a function of the source's mean number of photon pairs emitted from

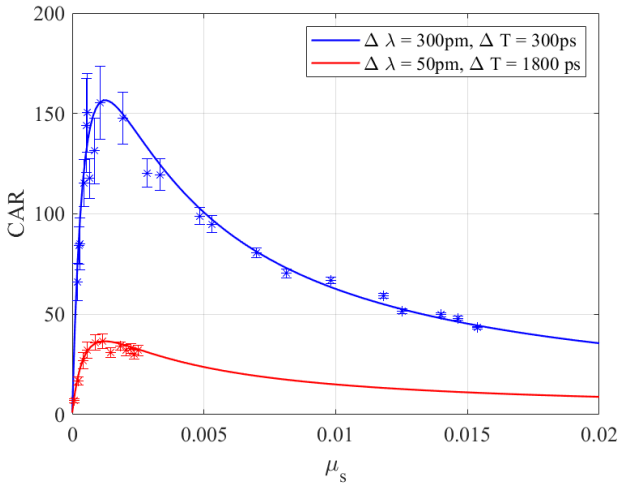

FIG. 4: CAR as a function of μ_s for two different cases that have the same single-channel time-frequency filtering product. The plot clearly shows a drastic reduction in CAR for the narrower spectral filtering case, even though the single-photon SNR in signal or idler detectors is equivalent for both cases. This shows a distinction between the behavior of single-photon filtering and filtering SPDC/SFWM sources.

the source, where we choose to plot as a function of the signal mode's mean number of photons mus.

Fig. 4 shows the results of the experiment. For this test, the C-band classical light source is set to obtain a received power at the end of the fiber of P_R = -28 dBm. The heralding efficiency over the 25-km fiber for $\Delta\lambda$ = 50 pm had significantly lower values ($\eta_A = 0.00278, 0.0224$) compared to $\Delta\lambda = 50$ pm (0.0143, 0.0171). Thus, we expect that 50-pm case should be significantly more impacted by the effects of narrowly filtering the source JSI. Fig. 4 shows a clear difference between the 50pm/1800ps and 300pm/300ps filtering approaches. For 300pm we achieve a maximum CAR $\sim$ 160, whereas 50-pm filtering case reaches only $\sim$40. This clearly shows that cutting into the JSI can negatively impact performance, notably sacrificing the spectral purity of the photons. To have high spectral purity, one thus takes a hit on CAR for this source. Notably, the single-channel SNR was the same for both cases due to the fixed single-detector time-bandwidth product. Due to this, there is a clear difference between the impact of narrowly filtering photon pairs compared to single photons.

We can also see the impact of multi-pair emission in Fig 4. Each obtains a maximum around $\mu \sim 10^{-3}$, which needs to be increased due to the need to overcome noise photon count rates. However, as the source intensity is increased, multi-photon pair emission begins to degrade CAR.

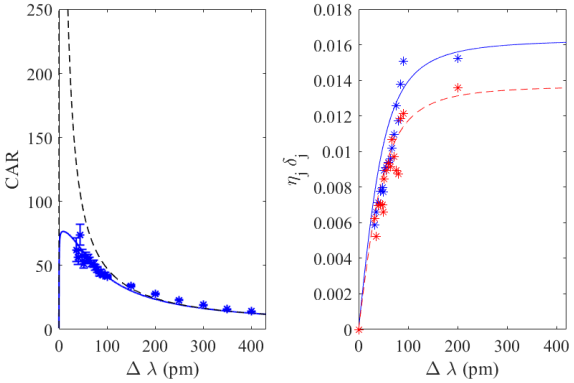

FIG. 5: (a) CAR for fixed EDFA pump power as the signal/idler filter bandwidths $\Delta\lambda$ are tuned whilst the classical channels transmit -12.5dBm of launch power into the 25km/25km spools. The black line shows the simulation using the ideal equations for CAR (ignoring the filtering of the JSA), and the blue line shows the simulation including reduced heralding efficiency at narrow $\Delta\lambda$. It is clear that the results deviate from the ideal case due to a reduced filter heralding efficiency as our filters cut into the source's JSA. (b) Measured and predicted filter heralding efficiency δ_j for signal-idler photons as a function of $\Delta\lambda$. The values are scaled to the heralding efficiency at wide bandwidths, which includes the "true" channel loss in our system η_s and η_i. It is clear that the results deviate from the ideal case when the heralding efficiency (spectral purity) begins to decrease (increase).

B. CAR versus filter bandwidth for fixed ΔT

Here we experimentally investigate the consequences of narrow spectral filtering around photon pairs to mitigate the impact of background noise photons. We pump our source with a single pulse to create correlated photon pairs with a pulse full-width at half maximum (FWHM) of 44 ps. The 10-Gbps C-band classical sources are set to have an equal launch power of $P_0 = -12.5$ dBm, which results in the SpRS noise count terms $\mathcal{R}_s$ = 1477.4 counts/pm/s and $\mathcal{R}_i$ = 1040.1 counts/pm/s. We use tunable bandwidth filters to evaluate CAR as a function of the signal/idler filter FWHM bandwidth $\Delta\lambda$ while we temporally filter with a fixed coincidence window of ΔT = 300ps. According to the measured JSI and theoretical predictions, the narrow filtering, $\Delta\lambda$ <100 pm, should begin to experience significant reductions in the filter heralding efficiency δ_j which is the regime of interest.

We fix the EDFA pump power to create a constant output source intensity per filter bandwidth. We note that due to this, the mean number of photons per pulse within $\Delta\lambda$ is varied, where we model the mean number of photons in each setting as $\mu_j(\Delta\lambda) \approx n_c\Gamma_j(\Delta\lambda)$. This

does not create a perfect comparison between each bandwidth setting due to the change in source intensity which varies the impact of multi-photon pair emission (see Section IV.B), but does allow us to experimentally confirm any deviation from the ideal model. The results for CAR vs. $\Delta\lambda$ are shown in Fig.5(a). We plot the model for both the ideal case (black dashed line) and using the model simulating the source JSA (blue line). Fig. 5(b) shows the measured and modeled reduction in heralding efficiency for each channel as we reduce the filter bandwidth, which is scaled to also account for the true channel efficiency η_j.

We observe that for $\Delta\lambda < 100$pm, the ability to improve CAR via spectral filtering becomes hindered by the reduction in heralding efficiency. This regime is near the regime in which $\tau_{pump} < \tau_{filt}$ where τ_{pump} is the temporal width of the source's pump pulse and τ_{filt} is the coherence time set by the filter bandwidth, which is the regime known to achieve higher $\mathcal{P}$. It is clear that as $\mathcal{P}$ is increased, the ability to increase noise tolerance is hindered. For example, if $\delta_j = 1$, then the ideal case predicts a $\mathrm{CAR}_{\mathrm{ideal}}(30\mathrm{pm}) \approx 155$, whereas the measured and predicted value accounting for $\delta_j < 1$ is $\mathrm{CAR}_{\mathrm{ideal}}(30\mathrm{pm}) \approx 70$, which is a significant deviation from the ideal case. This filter bandwidth gives a ratio between pump and filter coherence times of $\tau_{pump}/\tau_{filt} = 0.39$.

C. Optimizing source pumping and pair generation rate

The above experiment was conducted for a fixed EDFA pump power, meaning the mean number of photons per pulse $\mu(\Delta\lambda)$ varies as the bandwidth is changed. This does not provide an accurate comparison between spectral filtering settings since CAR is highly dependent on $\mu(\Delta\lambda)$ [19, 24]. In a noiseless environment, CAR is often approximated as $CAR \approx 1/\mu$, indicating quantum fidelity is always maximized as $\mu \to 0$ due to the minimization of multi-pair emission. However, when background noise is present, the value for μ which maximizes CAR must be increased due to the need to overcome the noise detection rates, but not too large so as to suffer from multi-pair noise. Thus, the optimal CAR will always be a balance between maximizing the ratio of source intensity to background noise intensity and reducing multi-pair emission noise. We expand this analysis to include modeling of the filtered source JSA to investigate the consequences of reduced coincidence probability.

Fig. 6 shows multiple simulations of CAR as a function of mean photon number for different pulse widths when the photons are filtered by a $\Delta\lambda = 30$, 100, or 500 pm FWHM Gaussian-shaped spectral filter for various different temporal pump pulse widths (τ) ranging from 5ps to 200ps FWHM. We also plot the idealized equation for CAR ($\delta = 1$) which neglects filtering of the JSA (black). We note that for each case we assume a 300ps coincidence window. This means that the detector's time-frequency filtering is not time-bandwidth limited in each channel showing a unique limitation of narrowly filtering photons in coincidence.

The first lesson from the simulations in Fig. 6 is that CAR is highly dependent on how the source is pumped, showing a unique property of filtering two-photon states generated by SPDC/SFWM. This is because as τ is decreased, the bandwidth in which a reduced coincidence probability occurs is wider than for a longer duration pump pulse. The reason for this can be seen in Fig. 6(d), which plots both δ_j and $\mathcal{P}$ as a function of pulse width for the three spectral filter bandwidth settings. It can be seen that for narrow filtering, such as $\Delta\lambda = 30$ pm, the value for $\delta_j(\tau_{\mathrm{pump}} = 5\mathrm{ps}) \ll \delta_j(\tau_{\mathrm{pump}} = 200\mathrm{ps})$ meaning there is a much higher probability to get a coincidence count for $\tau_{\mathrm{pump}} = 200$ps and thus a higher two-fold signal-to-noise ratio. However, the approach of maximizing τ_{pump} while minimizing $\Delta\lambda$ reduces the spectral purity of the photons showing a trade-off between quantum fidelity and the ability to achieve high-visibility HOM interference using these multi-mode photons, which is consequential for applications such as quantum teleportation or entanglement swapping in noisy environments.

In the above simulations, we evaluated a situation in which we have a fixed coincidence window of $\Delta T = 300$ps while varying the properties of the source (μ, $\Delta\lambda$, and τ_{pump}). However, using narrower pulses can allow for narrower temporal filtering around the pulses arriving at the detectors, so it is worthwhile to investigate tight temporal filtering around the pulses depending on their pulse duration. To account for this, we simulate CAR vs. μ and τ_{pump} for a variable coincidence window depending on the choice of pump and filter coherence times. In Fig. 6(b), we simulate using a coincidence window of $\Delta\mathrm{T}_j = \sqrt{\tau_{\mathrm{pump}}^2 + \tau_{\mathrm{filt}_j}^2}$, for $j = \{\mathrm{signal}, \mathrm{idler}\}$, which emulates the ability to filter narrower in the time domain depending on the choice of pump and filter setting. The above equation limits the minimum coincidence window to $\Delta T_{min_j} = \tau_{\mathrm{filt}_j}$ which we calculate assuming transform-limited Gaussian pulses with $\tau_{\mathrm{filt}_j} = 0.44 \times \lambda_j^2/(c\Delta\lambda_j)$, where λ_j is the filter's center wavelength and c is the speed of light in vacuum.

This simulation shows the interesting result that each choice of $\Delta\lambda$ can now achieve the same maximum CAR, however the behavior is still highly dependent on the pump pulse width for each case. In Fig. 6(d) we plot the maximum possible CAR that can be achieved for

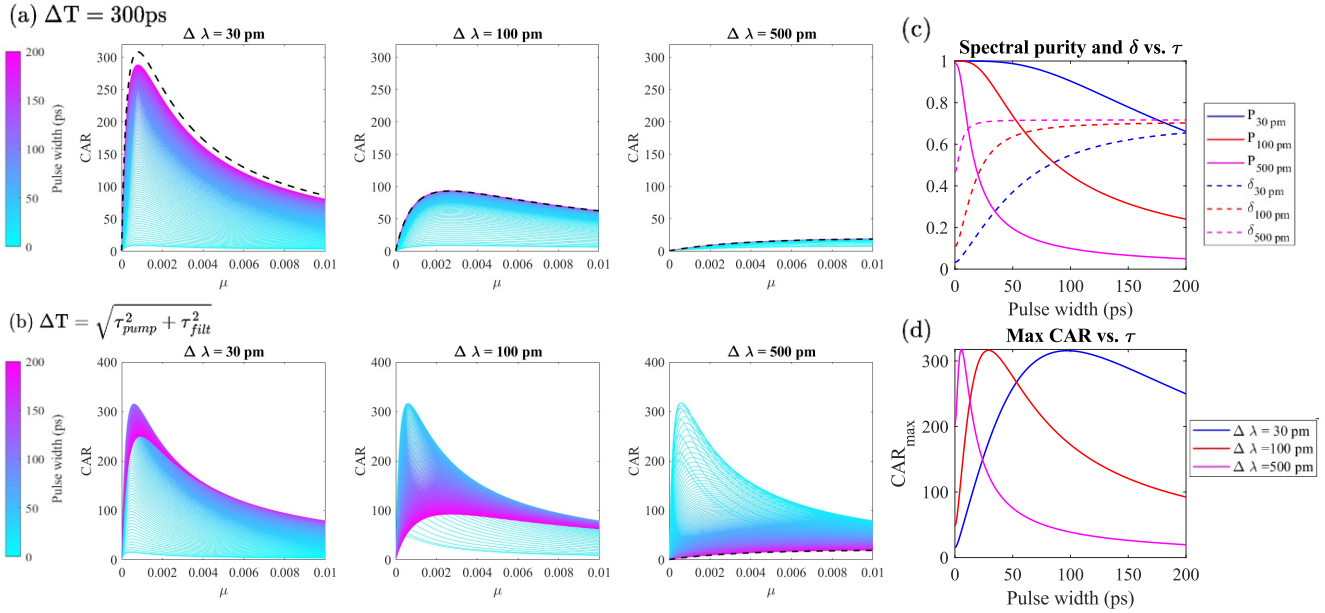

FIG. 6: (a) Simulated coincidence-to-accidental ratio (CAR) as a function of the mean number of photons per pulse within the signal/idler filter bandwidths μ for $\Delta\lambda = 30$ pm, 100 pm, or 500 pm when -12.5 dBm of C-band power is transmitted over 25-km/25-km fibers. We simulate the curve for various pump pulse widths from 5ps to 200ps. For this simulation we set a fixed coincidence window of $\Delta T = 300$ps for temporal filtering such that temporal filtering is never narrower than the photon's coherence times (not time-bandwidth limited).. The JSA is simulated for each different pump pulse width, with the black dashed line giving the ideal case of the filter heralding efficiency $\delta = 1$ regardless of the pump/filter bandwidths. The results clearly show a reduction in performance when using short pulses (light blue) compared to long pulses (purple). The plot shows that for typical sources, the optimal CAR is achieved using longer pulse widths and narrowband filtering. (b) Same simulation as in (a), but with an adjusted coincidence window such that using shorter pump pulses allows narrower temporal filtering. This result shows the ability to achieve the same maximum CAR, but the optimal pulse width different than in case (a). (c) Estimated spectral purity $\mathcal{P}$ (solid lines) and filter heralding efficiency (dashed lines) for each filter bandwidth as a function of pump pulse width, which helps relate the ability to perform multi-photon interference experiments to the ability to reject the impact of noise photons via filtering. (d) The maximum achievable CAR as a function of pump pulse width for the simulation in (b), demonstrating that each choice for $\Delta\lambda$ has a corresponding optimal pump pulse width.

each pump pulse width τ_{pump} for each $\Delta\lambda$ setting. It can be seen that for each setting of $\Delta\lambda$ there is a corresponding optimal τ_{pump}. The optimal choice seems to occur around $\tau_{pump} \approx \tau_{filt}$. This result would not occur if $\delta = 1$, indicating another consequence of reduced heralding efficiency when filtering photon pairs. It is also a unique property of photon-pair filtering, as the signal-to-noise ratio of single-photon filtering alone would not have a dependence on the pulse width at the transmitter.

The other lesson of the plot is that CAR is highly dependent on the mean photon number. It can be seen that as the noise is increased, the optimal CAR occurs at higher mean photon numbers but then degrades as multi-pair emission becomes a dominate source of noise.

V. C-BAND TIME-BIN ENTANGLEMENT COEXISTING WITH C-BAND CLASSICAL COMMUNICATIONS

Having explored filtering photon pair sources in various degrees of freedom, we now apply these to demonstrate a proof-of-principle application, namely entanglement-based networking coexisting with classical optical communications in fiber. We switch from generating single pulses at 200 MHz using the AWG to creating double pulses with a separation of 347 ps at the same repetition rate. At the receiver, we insert Michaelson interferometers to measure a non-local two-photon interference fringe in the Z basis. Although other entanglement distribution experiments coexisting with classical communications have been performed for polarization entanglement [4, 6, 7, 25] and time-energy entanglement [5], this is the first study of pulsed time-bin entanglement distribution over fibers populated with strong conventional

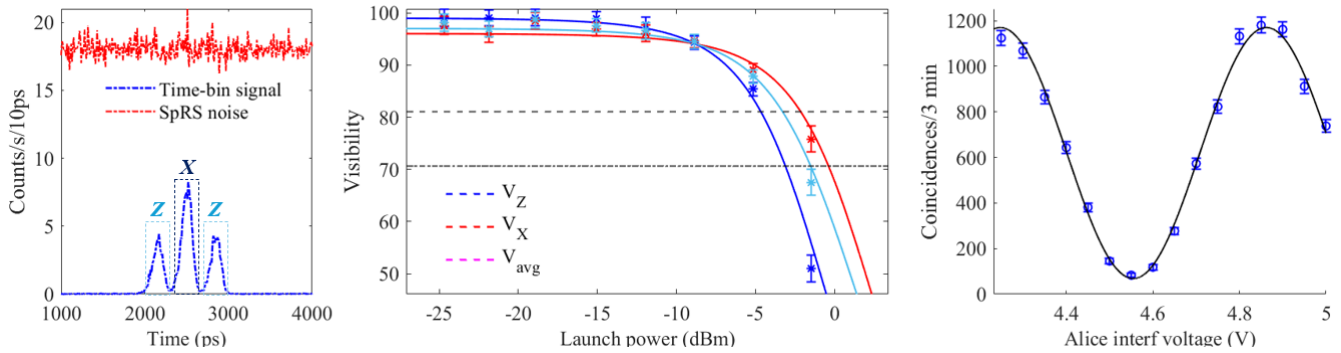

FIG. 7: C-band time-bin entanglement distribution coexisting over 25km/25km fibers with 10-Gbps co-propagating C-band classical data. (a) Histogram of single photon counts relative to our clock at the output of the signal photons interferometer when the classical launch power is -4.8 dBm. The blue shows the output from just our time-bin photons, showing the three peaks characteristic of sending time-bin entangled photons through a Michaelson interferometer. The red shows the SpRS background counts alone which are shown to have equal intensity across the three bins, with the side bins having a 2 times lower SNR compared to the middle bin. (b) Z-basis (blue), X-basis (red), and average (teal) entanglement visibility versus the C-band classical launch power. The two dashed lines show the minimum visibility for performing QKD (>81%) and verifying the non-local nature of entanglement (>70.7%). We observe that the X-basis is able to tolerate higher power and that our 50-pm/200-ps filtering enables classical power of -2.2 dBm to be tolerated. (c) Example non-local two-photon interference fringe by varying Alice's interferometer voltage, where we obtain a visibility of $V_X = 89.6 \pm 1.6\%$ at a launch power of $P_0 = -4.8$ dBm.

optical communications.

In this experiment, we choose to filter our photons at Bob and Charlie using 50-pm FWHM bandwidth spectral filtering applied to both photons (6.5 GHz) and apply 200-ps temporal filtering. The narrow filter bandwidth gives a ∼70ps photon coherence time, placing us close to the single-channel time-bandwidth limited filtering. The filter bandwidth is also very narrow relative to the width our JSI. This means we are in the regime of high spectral purity and low filter heralding efficiency, where we measure a reduction in heralding efficiency of approximately 23% and 21% for signal and idler photons going from 600pm to 50pm filtering, showing a significant reduction in the coincidence probability independent of the single-channel photon rate. At 50pm/50pm filtering, the true heralding efficiency was 0.0012 and 0.0014 for signal and idler, respectively. Converting between loss and fiber length, this corresponds to a total of approx. 300km standard fiber.

Fig. 7 shows the results of distributing our time-bin entangled pairs each over 25 km spools to co-propagate with 10-Gbps modulated C-band classical data signals. Fig. 7(a) shows a histogram of the signal photon singles count rate per 10 ps relative to our clock signal, which shows the three peaks at the output of our Michaelson interferometer. Note that our clock pulses have a frequency of 10MHz and the response rate of our laser pulses is 200MHz, so this histogram represents 1/20th of the single-photon singles data in a clock cycle. We also plot just the SpRS noise singles count rate on top of this when the classical signals are launching X and Y dBm into each fiber. This shows clearly that the SpRS noise is completely random in time, equal across the three bins. The side lobes of the quantum signal have 50% of the count rate compared to the middle peak, with a single-channel SNR of 0.41 and 0.205, respectively. This SNR is less than one, indicating the inability to perform quantum applications using the singles counts alone. However, thanks to the photon number correlations of entangled pairs, the vacuum component that is present in the single-channel measurements is less prominent when doing non-local coincidence detection, which makes the two-fold detection of the entangled state more robust against SpRS. However, the noise counts improperly herald the presence of the entangled pair, reducing the visibility alongside noise-noise two-fold coincidences.

Fig. 7(b) shows a plot of the Z (E/L) and X basis ($+/-$) visibility as we vary the launch power of the two classical signals into their respective fibers. In dark fiber, we measure visibility of $V_Z = 99.2\%$ and $V_X = 95.6\%$, where the X-basis visibility is slightly lower due to the imperfect visibility of our interferometers.

As we increase the launch power, we observed that V_Z declined more rapidly compared to V_X, which is due to the inherent properties of time-bin qubit analysis via interferometry. The $|E\rangle$ or $|L\rangle$ photons will exit the interferometer output randomly in each port 50% of the time, similar to adding 3-dB loss to the quantum signal. Simi-

larly, the noise will also randomly exit the interferometer, and thus also has a 3-dB loss passing through the interferometer. However, the qubits $|\pm\rangle$ and $|\pm i\rangle$ exit the interferometer output on the same side with 100% or 0% probability (neglecting any insertion loss). This creates three distinct satellite peaks in the histogram of single-photon detection times as seen in Fig. 7(a). Since the SpRS photons from the classical signal are entirely randomly distributed in time, the noise count probability across all peaks in the histogram are equal. This means that noise is reduced 50%, Z basis counts are reduced 50%, but $|\pm\rangle$ and $|\pm i\rangle$ states experience no loss (outside of insertion losses, which are applied to all). The states lying on the equator of the Bloch sphere are thus expected to significantly outperform states lying on the poles. This has consequences for all TF encodings such as time bins, frequency bins, and temporal modes. The coherence shared between the interfering bins enables constructive interference that helps push the coincidence signal above the noise. For many quantum applications, it is sufficient to observe only two mutually unbiased bases. In high-noise environments, this work shows that choosing encoding bases that utilize interference in their measurement such as $|\pm\rangle$ and $|\pm i\rangle$ instead of the more conventional Z basis choice can boost SNR and measurement visibility.

To time-bin entanglement, we change the equations for correlated pairs to include the additional loss of the photon pairs and noise counts, such that the coincidences and singles in the Z basis can be written as

$$C_{ee/ll} = \frac{1}{2}\Gamma_{both} n_c \eta_s \eta_i + S_s S_i \tag{5}$$

$$C_{el/le} = S_s S_i \tag{6}$$

$$S_j = \frac{1}{2}\Gamma_j n_c \eta_j + \left(\frac{1}{2}\mathcal{R}_j \Delta\lambda_j + d_j\right)\Delta T_j \tag{7}$$

For the X-basis, we model the coincidence counts as a function of phase between Alice and Bobs interferometers ϕ_{AB} can be expressed as:

$$C\left(\phi_{AB}\right) = \frac{\eta_s \eta_i}{2}\Gamma_{\text{both}} n_c \left(1 + V_{\text{int}} \cos\left(\phi_{AB}\right)\right) + A$$

giving the maximum and minimum coincidences of

$$C_{\max} = \frac{\eta_s \eta_i}{2}\Gamma_{\text{both}} n_c \left(1 + V_{\text{int}}\right) + S_s S_i$$

$$C_{\min} = S_s S_i + \frac{\eta_s \eta_i}{2}\Gamma_{\text{both}} n_c \left(1 - V_{\text{int}}\right)$$

$$S_j = \Gamma_j n_c \eta_j + \left(\frac{1}{2}\mathcal{R}_j \Delta\lambda_j + d_j\right)\Delta T_j \tag{8}$$

where V_{int} is the visibility of the interferometer.

From Fig. 7(b), we showed that the X basis visibility could reach the limit for QKD of V>81% at a launch power of -2.2 dBm (0.6 mW) and -0.4 dBm for violating Bell inequality [26], whereas the Z basis could only reach -4.4 dBm and -2.8 dBm, respectively. We also note that at the highest tested powers, our mean photon number was quite low, meaning we could have achieved higher powers if we were able to increase the source intensity to overcome the noise. We predict that by increasing μ by ∼3 times and temporally filtering down to 100-ps, we could achieve a visibility of >81% in the X basis with classical powers of > +2dBm.

In our experiment, our receiver required -18 dBm of power to operate the 10 Gbps communication error-free. Based on our maximum received power (0.16 mW), we predict that roughly 10 classical channels could have operated in a DWDM C-band classical system (100-Gbps total), assuming all operate at the minimum necessary classical power. We note, however, that much higher data rates as a function of classical power have been demonstrated in other experiments. For example, a common estimate for 10-Gbps error-free communications is a received power of -27 dBm [15], in which case 81 classical 10-Gbps channels (810 Gbps) could be populated in our system. More sophisticated methods for classical communications have been shown to allow even higher data rates. It was shown in [27] that sufficient powers were shown to be -50 dBm for PM-BPSK, -47 dBm for PM-QPSK and -38 dBm for PM-16QAM modulation formats. Classical data rates on the order of Tb/s have been demonstrated using single-photon QKD experiments alongside power levels similar to those of this study [28]. Furthermore, we have shown here an improvement of more than an order of magnitude in coexisting power compared to previous C-band/C-band entanglement distribution-classical studies [5].

We also note that this is an underestimation due to the C-band/C-band SpRS noise spectrum, since our quantum/classical wavelength allocation places our quantum center wavelength near the highest SpRS noise wavelength allocations [15, 28], where noise could have been roughly halved by placing the classical channel in the closest neighboring 100- or 50-GHz spaced DWDM channel.

VI. CONCLUSION AND OUTLOOK

In conclusion, we have studied various methods of filtering photon pair states generated from SPDC or SFWM sources, finding that performance is highly dependent on properties of the source's phase-matching conditions, pump spectral bandwidth, filter bandwidths, and pump power, which has broad implications for optimal source and receiver designs for multi-photon quantum applications in noisy environments.

We then demonstrated the coexistence of C-band time-bin-entangled photons coexisting with 10-Gbps C-band classical data. We found that the impact of SpRS has a basis-dependence on Michaelson interferometer-based time-bin measurements. Further, using narrow filtering, we demonstrated high C-band power levels over a total of 50 km of fiber. Although other approaches can be used for coexistence with classical data, such as allocating either the quantum [1, 4, 7, 29] or classical [16, 30–32] channels to the O-band, these results would allow entanglement-based networking and classical networks to both leverage the lower-loss C-band wavelengths.

We also note that these time-bin photons are spectrally pure, being forward compatible with applications such as teleportation coexisting with classical communications [7, 17] and are allocated to 1536.5 nm which are directly compatible with Er-ion QMs [33–35], offering insight into the challenges of operating at these wavelengths in coexisting advanced quantum-classical networks.

[1] P. D. Townsend, Electronics Letters **33**, 188 (1997), ISSN 0013-5194, publisher: Institution of Engineering and Technology.

[2] T. E. Chapuran, P. Toliver, N. A. Peters, J. Jackel, M. S. Goodman, R. J. Runser, S. R. McNown, N. Dallmann, R. J. Hughes, K. P. McCabe, et al., New Journal of Physics **11**, 105001 (2009), ISSN 1367-2630.

[3] Y. Mao, B.-X. Wang, C. Zhao, G. Wang, R. Wang, H. Wang, F. Zhou, J. Nie, Q. Chen, Y. Zhao, et al., Opt. Express **26**, 6010 (2018).

[4] J. M. Thomas, G. S. Kanter, and P. Kumar, Opt. Express **31**, 43035 (2023), URL https://opg.optica.org/oe/abstract.cfm?URI=oe-31-26-43035.

[5] Y.-R. Fan, Y. Luo, Z.-C. Zhang, Y.-B. Li, S. Liu, D. Wang, D.-C. Zhang, G.-W. Deng, Y. Wang, H.-Z. Song, et al., Phys. Rev. A **108**, L020601 (2023).

[6] R. Wang, R. Yang, M. J. Clark, R. D. Oliveira, S. Bahrani, M. Peranić, M. Lončarić, M. Stipčević, J. Rarity, S. K. Joshi, et al., in *49th European Conference on Optical Communications (ECOC 2023)* (Institution of Engineering and Technology, 2023), p. 1682 – 1685.

[7] J. M. Thomas, F. I. Yeh, J. H. Chen, J. J. Mambretti, S. J. Kohlert, G. S. Kanter, and P. Kumar, Optica **11**, 1700 (2024), URL https://opg.optica.org/optica/abstract.cfm?URI=optica-11-12-1700.

[8] C.-Z. Peng, T. Yang, X.-H. Bao, J. Zhang, X.-M. Jin, F.-Y. Feng, B. Yang, J. Yang, J. Yin, Q. Zhang, et al., Phys. Rev. Lett. **94**, 150501 (2005), URL https://link.aps.org/doi/10.1103/PhysRevLett.94.150501.

[9] Q. Lin, F. Yaman, and G. P. Agrawal, Phys. Rev. A **75**, 023803 (2007), URL https://link.aps.org/doi/10.1103/PhysRevA.75.023803.

[10] P. S. Kuo, J. S. Pelc, C. Langrock, and M. M. Fejer, Opt. Lett. **43**, 2034 (2018), URL https://opg.optica.org/ol/abstract.cfm?URI=ol-43-9-2034.

[11] Y. Yu, F. Ma, X.-Y. Luo, B. Jing, P.-F. Sun, R.-Z. Fang, C.-W. Yang, H. Liu, M.-Y. Zheng, X.-P. Xie, et al., Nature **578**, 240 (2020), ISSN 0028-0836, 1476-4687, URL https://www.nature.com/articles/s41586-020-1976-7.

[12] D. Lago-Rivera, J. V. Rakonjac, S. Grandi, and H. D. Riedmatten, Nature Communications **14**, 1889 (2023), ISSN 2041-1723, URL https://www.nature.com/articles/s41467-023-37518-5.

[13] M. L. H. Korsgaard, J. G. Koefoed, and K. Rottwitt, Phys. Rev. A **110**, 033508 (2024), URL https://link.aps.org/doi/10.1103/PhysRevA.110.033508.

[14] E. Meyer-Scott, N. Montaut, J. Tiedau, L. Sansoni, H. Herrmann, T. J. Bartley, and C. Silberhorn, Phys. Rev. A **95**, 061803 (2017), URL https://link.aps.org/doi/10.1103/PhysRevA.95.061803.

[15] P. Eraerds, N. Walenta, M. Legré, N. Gisin, and H. Zbinden, New Journal of Physics **12**, 063027 (2010), ISSN 1367-2630.

[16] A. Rahmouni, P. S. Kuo, Y. S. Li-Baboud, I. A. Burenkov, Y. Shi, M. V. Jabir, N. Lal, D. Reddy, M. Merzouki, L. Ma, et al., J. Opt. Commun. Netw. **16**, 781 (2024), URL https://opg.optica.org/jocn/abstract.cfm?URI=jocn-16-8-781.

[17] J. M. Thomas, F. I. Yeh, J. H. Chen, J. J. Mambretti, S. J. Kohlert, G. S. Kanter, and P. Kumar, in *Quantum Communications and Quantum Imaging XXIII* (SPIE, 2024), vol. 13391 of *Proceedings of SPIE*, pp. 13391–28, URL https://www.spie.org/photonics-west/presentation/Multiphoton-interference-and-quantum-teleportation-coex 13391-28.

[18] R. Ursin, F. Tiefenbacher, T. Schmitt-Manderbach, H. Weier, T. Scheidl, M. Lindenthal, B. Blauensteiner, T. Jennewein, J. Perdigues, P. Trojek, et al., Nature Physics **3**, 481 (2007), ISSN 1745-2481, URL https://doi.org/10.1038/nphys629.

[19] H. Takesue and K. Shimizu, Optics Communications **283**, 276 (2010), ISSN 00304018.

[20] C. I. Osorio, N. Sangouard, and R. T. Thew, Journal of Physics B: Atomic, Molecular and Optical Physics

46, 055501 (2013), URL https://dx.doi.org/10.1088/0953-4075/46/5/055501.

[21] E. Meyer-Scott, N. Montaut, J. Tiedau, L. Sansoni, H. Herrmann, T. J. Bartley, and C. Silberhorn, Phys. Rev. A **95**, 061803 (2017), URL https://link.aps.org/doi/10.1103/PhysRevA.95.061803.

[22] A. Mueller, S. I. Davis, B. Korzh, R. Valivarthi, A. D. Beyer, R. Youssef, N. Sinclair, C. Peña, M. D. Shaw, and M. Spiropulu, Optica Quantum **2**, 64 (2024).

[23] J. C. Chapman, J. M. Lukens, M. Alshowkan, N. Rao, B. T. Kirby, and N. A. Peters, Phys. Rev. Appl. **19**, 044026 (2023).

[24] M. Takeoka, R.-B. Jin, and M. Sasaki, New Journal of Physics **17**, 043030 (2015), URL https://dx.doi.org/10.1088/1367-2630/17/4/043030.

[25] C. Liang, K. F. Lee, J. Chen, and P. Kumar, in *2006 Optical Fiber Communication Conference and the National Fiber Optic Engineers Conference* (2006), pp. 1–3.

[26] J. F. Clauser, M. A. Horne, A. Shimony, and R. A. Holt, Physical Review Letters **23**, 880 (1969), ISSN 0031-9007.

[27] M. Mlejnek, N. A. Kaliteevskiy, and D. A. Nolan, *Reducing spontaneous raman scattering noise in high quantum bit rate qkd systems over optical fiber* (2017), 1712.05891, URL https://arxiv.org/abs/1712.05891.

[28] T. Dou, R. Liu, S. Liao, J. Tang, J. Tong, R. Ma, Y. Wan, R. Wang, J. Wu, X. Zhang, et al., Opt. Express **32**, 28356 (2024), URL https://opg.optica.org/oe/abstract.cfm?URI=oe-32-16-28356.

[29] L.-J. Wang, K.-H. Zou, W. Sun, Y. Mao, Y.-X. Zhu, H.-L. Yin, Q. Chen, Y. Zhao, F. Zhang, T.-Y. Chen, et al., Phys. Rev. A **95**, 012301 (2017).

[30] K. Kapoor, S. Xie, J. Chung, R. Valivarthi, C. Pena, L. Narvaez, N. Sinclair, J. P. Allmaras, A. D. Beyer, S. I. Davis, et al., IEEE Journal of Quantum Electronics pp. 1–1 (2023), ISSN 0018-9197, 1558-1713.

[31] J. M. Thomas, G. S. Kanter, S. Xie, J. Chung, R. Valivarthi, C. Peña, R. Kettimuthu, P. Spentzouris, M. Spiropulu, and P. Kumar, in *Optical Fiber Communication Conference (OFC) 2023* (Optica Publishing Group, 2023), p. Tu3I.3.

[32] I. A. Burenkov, A. Semionov, Hala, T. Gerrits, A. Rahmouni, D. Anand, Y.-S. Li-Baboud, O. Slattery, A. Battou, and S. V. Polyakov, Opt. Express **31**, 11431 (2023).

[33] F. Bussières, C. Clausen, A. Tiranov, B. Korzh, V. B. Verma, S. W. Nam, F. Marsili, A. Ferrier, P. Goldner, H. Herrmann, et al., Nature Photonics **8**, 775 (2014), ISSN 1749-4885, 1749-4893, URL https://www.nature.com/articles/nphoton.2014.215.

[34] M.-H. Jiang, W. Xue, Q. He, Y.-Y. An, X. Zheng, W.-J. Xu, Y.-B. Xie, Y. Lu, S. Zhu, and X.-S. Ma, Nature Communications **14**, 6995 (2023), URL https://www.nature.com/articles/s41467-023-42741-1.

[35] Y.-Y. An, Q. He, W. Xue, M.-H. Jiang, C. Yang, Y.-Q. Lu, S. Zhu, and X.-S. Ma, arXiv preprint arXiv:2505.05233 (2025), URL https://arxiv.org/abs/2505.05233.

Appendix A: Model for incorporating JSA

In the above analysis, we either model the effects of filtering the two-photon spectral correlations using numerical calculation of the filter heralding efficiency and spectral purity, a Gaussian approximation for the JSA, or experimentally measured using values.

The JSA of an arbitrary source can be constructed by using the general equation [14]

$$\begin{aligned} f(\omega_s,\omega_i) =& N \exp\left(\frac{-(\omega_s-\omega_{s0}+\omega_i-\omega_{i0})^2}{4\sigma_p^2}\right) \\ & \times \operatorname{sinc}\left(\frac{([\omega_s-\omega_{s0}]\sin\theta+[\omega_i-\omega_{i0}]\cos\theta)}{2\sigma_{pm}}\right) \end{aligned} \tag{A1}$$

Here, σ_p is the pump spectral bandwidth, σ_{pm} is the phase matching bandwidth, and $\theta = \arctan\left(\frac{k_p'-k_s'}{k_p'-k_i'}\right)$ is the phase-matching angle, where k_x' is the frequency derivative of k of the signal or idlers.

Applying spectral filtering effectively truncates the JSA, creating a new shape for the two-photon correlation. The new JSA can be obtained by multiplication with the transmission functions of the filters, giving the equation [14]

$$|\psi\rangle = \iint d\omega_s d\omega_i f(\omega_s,\omega_i)\, g_s(\omega_s)\, g_i(\omega_i)\, |\omega_s\rangle\, |\omega_i\rangle$$

where $|\omega_s\rangle$ and $|\omega_i\rangle$ are single photons at frequency ω_s and ω_i and $g_s(\omega_s)$ and $g_i(\omega_i)$ are spectral filters on the signal and idler photons, respectively.

When we apply the Gaussian approximation for the JSI, we use the method in ref. [14, 20]. Using some assumptions, it allows modeling an arbitrary Gaussian photon-pair joint spectrum filtered by Gaussian signal and idler filters. The filters have central frequencies of $\omega_{s0/i0}$ (units of rad Hz), and the bandwidths of the pump and phase matching are (σ_p) and (σ_{pm}), respectively. These are related to the FWHM bandwidth by

$$\begin{aligned} &\sigma_p = \sigma_{p_{FWHM}}/(2\sqrt{2\ln 2}) \approx 0.425\sigma_{p_{FWHM}}, \\ &\sigma_{pm} = \sqrt{0.193}\sigma_{p_m m_{FHM}}/(2\sqrt{2\ln 2}) \approx 0.187\sigma_{pm_{FWHM}} \end{aligned} \tag{A2}$$

To find the probability that both photons pass their filters, then the probability that each photon is passed individually. The unfiltered state is given by $|\psi\rangle = \iint d\omega_s d\omega_i f(\omega_s,\omega_i)\,|\omega_s\rangle\,|\omega_i\rangle$ with

$$\begin{aligned} \Gamma_{unfilt} &= |\langle\psi \mid \psi\rangle|^2 \\ &= \iint d\omega_s d\omega_i \left|f(\omega_s,\omega_i)\right|^2 \equiv 1 \end{aligned}$$

To obtain an analytical expression, we use the approximate sinc(x) $\approx \exp\left(-\alpha x^2\right)$ with $\alpha = 0.193$ for the JSA and then add Gaussian filters to signal and idler photons with bandwidths of $\sigma_{s/i} = \sigma_{s/i_{FWHM}}/(2\sqrt{2\ln 2})$. Neglecting phase contributions, this gives the filtered JSA of

$$\begin{aligned} f(\omega_s,\omega_i)\,\mathcal{F}_s(\omega_s)\,\mathcal{F}_i(\omega_i) &\approx N\exp\left(-\frac{(\Omega_s+\Omega_i)^2}{4\sigma_p^2}\right) \\ &\times \exp\left(\frac{-\alpha\left(\Omega_s\sin\theta+\Omega_i\cos\theta\right)^2}{4\sigma_{pm}^2}\right) \\ &\times \exp\left(-\frac{\Omega_s^2}{4\sigma_s^2}-\frac{\Omega_i^2}{4\sigma_i^2}\right) \end{aligned} \tag{A3}$$

where

$$f(\omega_s,\omega_i) \approx N\exp\left(-\frac{a}{4}\Omega_s^2-\frac{b}{4}\Omega_i^2-\frac{c}{2}\Omega_s\Omega_i\right) \tag{A4}$$

and

$$\begin{aligned} a &= \frac{\alpha^2\sin^2\theta}{\sigma_{pm}^2}+\frac{1}{\sigma_p^2}+\frac{1}{\sigma_s^2} \\ b &= \frac{\alpha^2\cos^2\theta}{\sigma_{pm}^2}+\frac{1}{\sigma_p^2}+\frac{1}{\sigma_i^2} \\ c &= \frac{\alpha^2\cos\theta\sin\theta}{\sigma_{pm}^2}+\frac{1}{\sigma_p^2} \end{aligned} \tag{A5}$$

The coincidence count probability can be found by setting $\frac{1}{\sigma_s^2} = \frac{1}{\sigma_i^2} = 0$ in equation A5 to obtain

$$\Gamma_{\text{unfilt}} = N^2\iint d\Omega_s d\Omega_i \exp\left(-\frac{a_0}{2}\Omega_s^2-\frac{b_0}{2}\Omega_i^2-c\Omega_s\Omega_i\right) \tag{A6}$$

where N^2 is a normalizing factor given by

$$N^2 = \frac{\sqrt{a_0b_0-c^2}}{2\pi} \tag{A7}$$

The coincidence probability for the filtered JSA is then

$$\begin{aligned} \Gamma_{\text{both}} &= N^2\iint d\Omega_s d\Omega_i \exp\left(-\frac{a}{2}\Omega_s^2-\frac{b}{2}\Omega_i^2-c\Omega_s\Omega_i\right) \\ &= \sqrt{\frac{a_0b_0-c^2}{ab-c^2}}. \end{aligned} \tag{A8}$$

Setting one of the signal or idler filter bandwidths to infinity gives the marginal probabilities for each individual photon, giving the single-channel probabilities of

$$\begin{aligned} \Gamma_i &= \sqrt{\frac{a_0b_0-c^2}{a_0b-c^2}} \\ \Gamma_s &= \sqrt{\frac{a_0b_0-c^2}{ab_0-c^2}} \end{aligned} \tag{A9}$$

To obtain the filter heralding efficiency $\delta_{s/i}$ we then take the ratio of the coincidence and single-channel probabilities to get

$$\begin{aligned} \delta_s &= \frac{\Gamma_{\text{both}}}{\Gamma_i} = \sqrt{\frac{a_0b-c^2}{ab-c^2}} \\ \delta_i &= \frac{\Gamma_{\text{both}}}{\Gamma_s} = \sqrt{\frac{ab_0-c^2}{ab-c^2}}. \end{aligned} \tag{A10}$$

To find the purity $\mathcal{P}$ we need the reduced density matrix for heralded signal or idler photons. Since our photons are entangled only in the spectral degree of freedom and we consider the case when both photons are detected, we assume each will have the same purity meaning calculating the purity of either reduced density matrix is sufficient. Neglecting the higher-order photon pair terms and vacuum component, obtain the reduced density matrix

$$\begin{aligned} \rho_s &= \text{Tr}_i(|\psi\rangle\langle\psi|) \\ &= \iiint d\Omega_i d\Omega_s d\Omega_s' f(\Omega_s,\Omega_i)\,f^*(\Omega_s',\Omega_i)\,|\Omega_s\rangle\langle\Omega_s'| \end{aligned} \tag{A11}$$

The spectral purity $\mathcal{P}$ can then be estimated using the Gaussian approximation for the JSA to be

$$\begin{aligned} \mathcal{P} &= \text{Tr}\left(\rho_s^2\right) \\ &= \iiint\int_0 d\Omega_s d\Omega_s' d\Omega_i d\Omega_i' \\ &\times f(\Omega_s,\Omega_i)\,f^*(\Omega_s',\Omega_i)\,f(\Omega_s',\Omega_i')\,f^*(\Omega_s,\Omega_i') \\ &= N^4\frac{(2\pi)^2}{\sqrt{a^2b^2-abc^2}} \\ &= \sqrt{\frac{(ab-c^2)^2}{a^2b^2-abc^2}} \\ &= \sqrt{\frac{ab-c^2}{ab}} \end{aligned} \tag{A12}$$

Appendix B: Time filtering

In this section we investigate temporal filtering of our correlated photon pairs. We fix the filter bandwidth at $\Delta\lambda$ =100pm and test CAR as a function of

ΔT =10ps to 600ps. We investigate two different pump pulse widths, namely τ_{pump} = 50ps and 320ps to determine if there is any difference in filtering the two sources. The noise count rates in the 100pm filter bandwidths were 1.84×10^6 and 1.81×10^6 counts/s in signal and idler channels, respectively. For this case, the 100pm filters were Fabry-Perot etalon filters with 100-GHz free-spectral range to allow filtering with the 100-GHz channel spacing DWDMs used to multiplex quantum and classical channels. Since these have much lower insertion loss compared to the tunable bandwidth filters, we have a higher true channel efficiency of $\eta_s = 0.024$ and $\eta_i = 0.027$.

Fig. 8(a) shows CAR as a function of coincidence window for the two pulse width cases and Fig. 8(b) shows the measured coincidence count rates as we reduce the coincidence window. The reduction in coincidence counts as we go below $\Delta T \approx 200$ps is due to cutting into the pulse width.

The mean photon number for each case was measured to be $\mu_{320ps} \approx 0.011$ and $\mu_{50ps} \approx 0.0097$ for the long and short pulse case, respectively. Since these have different mean photon numbers it does not give an exact comparison between the two cases but does allow us to evaluate any potential difference in trends between the two cases with narrow temporal filtering. The solid lines in Fig. 8(a) show the predictions if we assume that mu is kept constant and noise is reduced linearly with and without reduction in coincidence probability (assuming Fig. 8(b) were a constant line as a function of ΔT).

Fig. 8(a) shows that for each case, reducing the coincidence window can significantly improve CAR, as expected. However, both cases seem to stop improving at a similar limit which is roughly $\Delta T < 100$ps. We predict that this is likely due to the jitter of our SNSPDs and time-taggers starting to contribute to the inability to truly reduce the coincidence detection window.

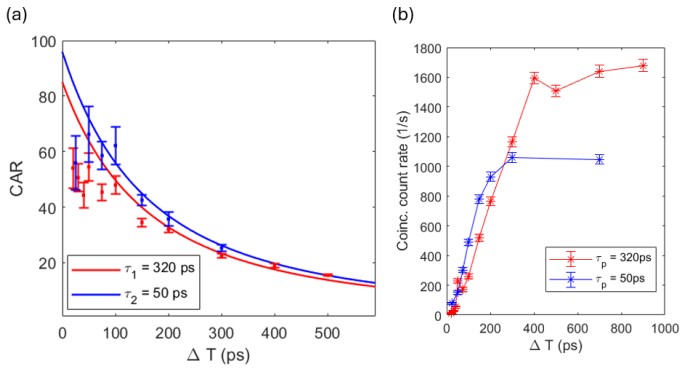

FIG. 8: (a) CAR versus coincidence window ΔT for a source pumped by a 50 ps pump pulse (blue) and a 320 ps (red) pulse when the photons are spectrally filtered by a $\Delta\lambda = 100$ pm filter. The classical received power was $P_R = -17.7$ dBm. The solid lines show the prediction if we assume the noise counts were reduced linearly and coincidence counts remained constant. (b) Coincidence count rate as a function of ΔT.

It is also true that narrow temporal filtering relative to the photon filter coherence time τ_{filt} can be a way to increase $\mathcal{P}$ (instead of using a short pump pulse) [21]. In this case, we would expect to see similar reduction in heralding efficiency as we saw in the spectral filtering case due to cutting into the joint temporal amplitude (JTA), which is the Fourier transform of the JSA. If we let the spectrally filtered JSA be $\Phi(\omega_s, \omega_i) = f(\omega_s, \omega_i)\, g_s(\omega_s)\, g_i(\omega_i)$, where g are the filter spectral functions, then the JTA can be written as the Fourier transform of the JSA $\mathcal{F}[\Phi(\omega_s, \omega_i)]$. If we apply some time filters $T_j(t)$ to the photon pairs, then we can write the effect of time-filtering the JSA as $\Phi(\omega_s, \omega_i)_{\Delta T} = \mathcal{F}^{-1}[T_s(t) T_i(t')] * \Phi(\omega, \omega')$. It is clear that time-filtering could lead to a similar enhancement in $\mathcal{P}$, but also results in a reduction in δ_j due to the emission of temporal modes in the coincidence window at incompatible times to give coincidences between signal/idler photons. This will also lead to a reduction in the ability to improve. However, since our detector jitter is one the order of $\sim$ 50ps, this limitation is more pronounced compared to the spectral filtering case and has a large contribution in the narrow filtering regime in Fig. 8(a), which is why we predict this is a main reason for a limited ability to maximize performance at $<$ 50ps, even with the short pump pulse system.

Appendix C: Visibility versus source phase-matching angle

Here we investigate properties of the phase-matching of the source. This could be insightful due to the fact that the impact of heralding efficiency on either signal or idler photons

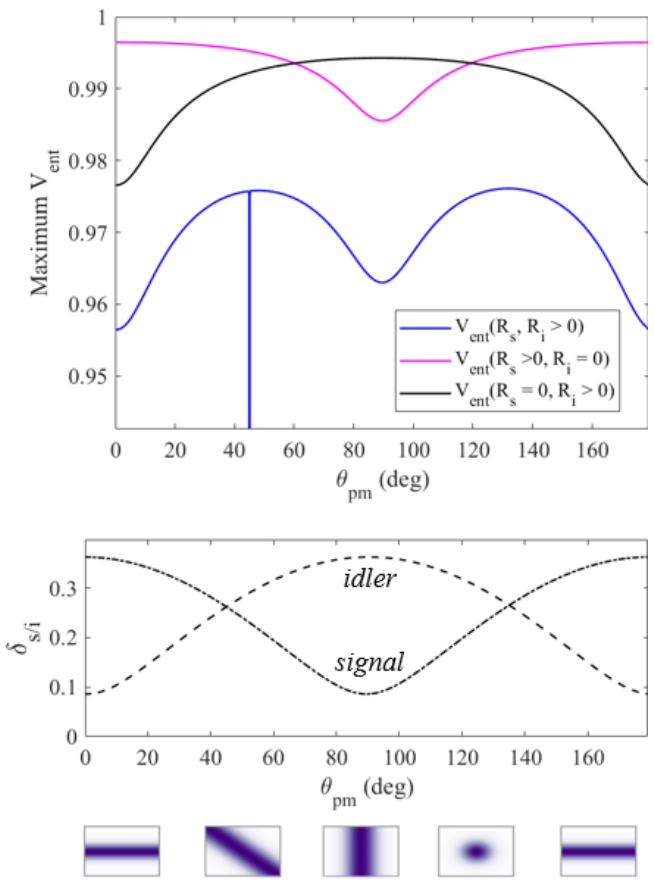

FIG. 9: (a) Maximum possible visibility versus the source's phase-matching angle for $P_0 = -12$dBm. We consider three cases, one where both photons are sent over the noisy medium, one where only the signal photon detector has noise, and one where only the idler detector has noise. (b) The signal and idler heralding efficiencies as a function of phase-matching angle. The pump pulse width is set to $\tau_{pump} = 20$ps and $\Delta\lambda = 100$pm. The bottom shows the shape of the JSA for each θ_{pm}.

Appendix D: Polarization filtering

Here we investigate the consequences of polarization filtering unpolarized noise, which is common in both quantum-classical coexistence in optical fiber and in free-space communications, polarization filtering can roughly halve the amount of noise in each detector. For free space systems, this can be relatively more stable, however optical fibers are susceptible to polarization drift over time due to time-dependent temperature and mechanical stress fluctuations. Even in dark fiber, such rotations can be catastrophic to quantum encoding in polarization. Ignoring noise, the fidelity of spectral or temporal qubits is not impacted by polarization drift. However, if one uses polarization filtering to reduce noise, one still needs to compensate for fiber drift or else the polarized quantum signal rates, partially blocked by the polarizing element, become reduced relative to unpolarized noise, which stays constantly at $\mathcal{R}/2$.

To evaluate this experimentally, we transmit polarized photon pairs over 25km optical fibers to coexist with a classical communications signal that is generating noise that is unpolarized via spontaneous Raman scattering. Due to polarization mode dispersion, the noise is mostly randomly polarized at the end of long-distance fiber. We let both 25km fibers experience significant polarization drift over time, starting with the signal aligned to a PBS to achieve the maximum CAR, then seeing how this is degraded as a function of time as the polarization drifts away from the optimal angle relative to the polarizer. Fig. 10(a) shows the singles count rates in channel A and B, which shows that the SpRS noise rates remain constant over time whereas the photon pair rates are reduced over time and thus the SNR in each channel is degraded. Fig. 10(b) shows CAR as a function of the same time interval, clearly showing a reduction as the angle of the quantum signal $\theta_{s,i}$ drifts from the polarizer angle θ_{pol}. We also model CAR as a function of time using a time dependent channel efficiency for the quantum signal $\eta_j \rightarrow \eta_j \cos^2(\theta_{pol} - \theta_j)$ while keeping noise count probability of $\mathcal{R}/2$. This indicates that active polarization tracking is extremely important in noisy environments, even for qubit encoding that is otherwise not impacted (in terms of fidelity) by polarization drift in noiseless fibers.

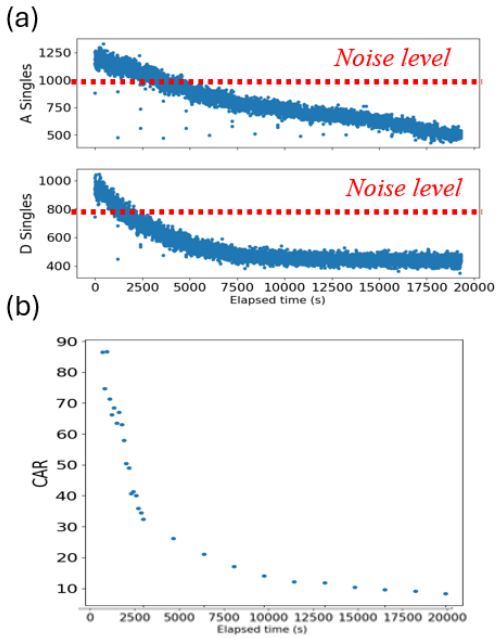

FIG. 10: Polarization filtering: (a) Singles counts as a function of time for transmission over a fiber with unpolarized noise with time-varying birefringence that is uncompensated. The noise level stays constant at $\mathcal{R}/2$ due to the polarizer, but time-dependent polarization rotations reject the quantum signal with polarization dependent efficiency $\eta_j(\theta_j)$. (b) CAR as a function of time, showing reduction in CAR when polarization is not compensated over time.